

Towards more accurate First Principles prediction of redox potentials in transition-metal compounds with LDA+U

F. Zhou

Department of Physics, Massachusetts Institute of Technology, Cambridge, MA 02139

M. Cococcioni, C. A. Marianetti, D. Morgan, G. Ceder

Department of Material Science and Engineering,

Massachusetts Institute of Technology, Cambridge, MA 02139

(Dated: February 8, 2020)

Abstract

First-principles calculations within the Local Density Approximation (LDA) or Generalized Gradient Approximation (GGA), though very successful, are known to underestimate redox potentials, such as those at which lithium intercalates in transition metal compounds. We argue that this inaccuracy is related to the lack of cancellation of electron self-interaction errors in LDA/GGA and can be improved by using the DFT+*U* method with a self-consistent evaluation of the *U* parameter. We show that, using this approach, the experimental lithium intercalation voltages of a number of transition metal compounds, including the olivine Li_xMPO_4 (M=Mn, Fe Co, Ni), layered Li_xMO_2 ($x = \text{Co, Ni}$) and spinel-like $\text{Li}_x\text{M}_2\text{O}_4$ (M=Mn, Co), can be reproduced accurately.

PACS numbers: 71.15.Nc, 71.27.+a, 82.47.Aa

I. INTRODUCTION

Redox processes are relevant to many technological applications, including corrosion, fuel cells and rechargeable Li batteries, and the ability to study these processes with first principles method is therefore crucial. The key to a redox reaction is the transfer of electrons from one species to another. When the redox electron is transferred between very distinct environments (e.g. metallic to ionic) the standard Local Density Approximation (LDA) and Generalized Gradient Approximation (GGA) lead to considerable errors in the calculated redox energies. We show in this paper that treating self-interaction with the DFT+ U ^{2,3} method gives considerably better agreement with experiment and thereby provides a tool to accurately predict redox potentials.

The particular problem we study with GGA and GGA+ U is that of Li insertion in transition metal compounds. Transition metal (TM) compounds have attracted intense research as cathode materials for rechargeable Li batteries due to their ability to simultaneously absorb Li⁺ ions and electrons. In the discharge cycle of a rechargeable battery Li is oxidized on the anode side and inserted as Li⁺ + e⁻ in the TM compound that comprises the cathode. The energy of this reaction determines the oxidization/reduction potential at which the battery operates. It is the high redox potential of Li cells that makes them so desirable in applications where high energy density is required.

First principles calculations have been used extensively to predict important properties of Li-insertion materials such as the average potential^{4,5,6,7,8,9,10,11,12,13,14} and potential profile^{15,16} for Li insertion, phase stability^{17,18,19} and Li diffusion²⁰. While this has led to considerable success in predicting the trends of Li insertion voltages⁴ and even new phases¹⁵, it has been noted that LDA and GGA can give relatively large errors for the average Li insertion potential^{4,21}. For example, Table I compares the experimental voltage for different structures with the one calculated in the GGA approximation and with computational details discussed in section III. The Li insertion potential is consistently underpredicted by as

	LiNiO ₂ /NiO ₂	LiMn ₂ O ₄ /Mn ₂ O ₄	LiFePO ₄ /FePO ₄
GGA	3.19	3.18	2.97
exp.	3.85 ²²	4.15 ²³	3.5 ²⁴

TABLE I: Calculated and experimental redox couple voltage in Volt.

much as 0.5 to 1.0V. Similar results have been obtained with LDA⁴.

Recently, we have shown that electron correlation plays an important role in predicting the phase diagram of the Li_xFePO_4 system²⁵, for which LDA and GGA qualitatively fail. In this work we demonstrate that the DFT+*U* method also corrects the voltage error from LDA and GGA. In our approach, *U* is calculated self-consistently²⁶, thereby making this a “first-principles” approach to predict redox potentials with no adjustable parameters.

We first present some background information on the specific Li insertions materials investigated and how the electrochemical reactions take place in a rechargeable lithium battery. We also discuss the details of the DFT+*U* method and the self-consistent calculation of *U*. In Sec. III we show the results of our approach, highlighting the improvement over GGA and the good agreement with experiment.

II. MATERIALS AND METHODOLOGY

A. Materials and Crystal structures

As a representative set of Li-insertion compounds, we have picked a few materials that represent different environments for the Li and TM ions, and which are well characterized experimentally.

The family LiMPO_4 of olivine structures (M=Mn, Fe, Co and Ni) has recently attracted much attention as a potential candidate for rechargeable Li-battery electrodes in large applications such as electric and hybrid vehicles²⁷. Olivine-type LiMPO_4 and the de-lithiated structure MPO_4 , have an orthorhombic unit cell with four Formula Units (FU) and space group Pnma (see Fig. 1). The olivine structure can be thought of as a distorted hexagonal close-packing of oxygen anions, with three types of cations occupying the interstitial sites: 1) Transition metals M in corner-sharing MO_6 octahedra which are nearly coplanar to form a distorted 2-d square lattice perpendicular to the **a** axis, 2) Lithium ions in edge-sharing LiO_6 octahedra aligned in parallel chains along the **b** axis, and 3) P ions in tetrahedral PO_4 groups connecting neighboring planes or arrays. It is believed that the PO_4 groups hybridize less with the TM than an oxygen anion does in simple close-packed oxides, and hence leads to more localized 3d states on the TM than in an oxide.

The layered LiMO_2 and spinel-like $\text{Li}_x\text{M}_2\text{O}_4$ are more traditional cathode materials that

have been thoroughly studied experimentally²⁸ and theoretically^{4,5,19,20}. They are both ordered rock salts (see Figs. 2, 3). The layered structure can be envisioned as two interpenetrating fcc lattices, one consisting of oxygen, and the other consisting of alternating (111) planes of Li and TM. In the $\bar{R}\bar{3}m$ space group the Li and the metal ions remain fixed in the ideal rock salt positions, but the whole (111) oxygen planes can relax in the [111] direction. The spinel-like structure $\text{Li}_x\text{M}_2\text{O}_4$ is so named because at $x = 1$ it has the same structure as the spinel mineral MgAl_2O_4 . We shall refer to it as spinel even when $x = 2$. It can be envisioned as a fcc oxygen sublattice, with TM in half of the octahedral oxygen interstices, and lithium either in part of the tetrahedral sites at $x = 1$ or in the octahedral sites not occupied by the TM ions for $x = 2$ ²⁸.

B. Relation between insertion voltage and total energies

When Li is inserted into a TM-oxide, its charge is compensated by an electron absorbed from the external circuit. The insertion reaction is symbolized by the following equation:



where MO_y is the TM compound host material. Using thermodynamical arguments, it is possible to relate the voltage V of the cell to the lithium chemical potential (μ_{Li}) on both sides of Eq. 1 in the cathode²⁹:

$$V(x) = -\frac{\mu_{\text{Li}(x)}^{\text{cathode}} - \mu_{\text{Li}}^{\text{anode}}}{F}. \quad (2)$$

F is the Faraday constant, and $\mu_{\text{Li}}^{\text{anode}}$ is the chemical potential in the anode, or more generally, the chemical potential of the Li source.

The average voltage $\langle V \rangle$ for Li insertion between two composition limits, $\text{Li}_{x_1}\text{MO}_y$ and $\text{Li}_{x_2}\text{MO}_y$, can be found by integrating Eqn. 2⁴ (usually between $x = 0$ and 1), and is determined by the free energy of the compounds at the composition limits. Neglecting the entropic and $P\Delta V$ contributions⁴ $\langle V \rangle$ can simply be determined by computing the total energy of $\text{Li}_{x_2}\text{MO}_y$, $\text{Li}_{x_1}\text{MO}_y$ and Li:

$$\langle V \rangle = \frac{[E(\text{Li}_{x_2}\text{MO}_y) - E(\text{Li}_{x_1}\text{MO}_y) - (x_2 - x_1)E(\text{Li metal})]}{(x_2 - x_1)F}. \quad (3)$$

Typically $x_1 = 0$ and $x_2 = 1$ are taken as composition limits, as in these cases one does not have to account for Li-vacancy disorder.

Experimentally, the voltage vs. lithium composition curve $V(x)$ can be conveniently measured for both the charging and discharging process. The charging and discharging curves differ in general because of the overcharge potential present in the circuit. We obtain the experimental average open circuit voltage values by numerically averaging the charge and discharge curves published in Refs. 22,23,24,30,31,32 over the appropriate composition range.

C. The DFT+U method

The DFT+U method, developed in the 1990's^{1,2,3}, is now a well-established model to deal with electron correlation in TM and rare earth compounds. The method combines the high efficiency of DFT+LDA/GGA, and an explicit treatment of correlation with a Hubbard like model for a subset of states in the system. To investigate whether the underestimation of the lithium intercalation voltage in LDA/GGA could be related to Coulombic on-site effects we carried out rotationally invariant DFT+ U ³ calculations. The essence of the method can be summarized by the expression for the total energy

$$E_{\text{LDA+U}}[\rho, \hat{n}] = E_{\text{LDA}}[\rho] + E_{\text{Hub}}[\hat{n}] - E_{\text{dc}}[\hat{n}] \equiv E_{\text{LDA}}[\rho] + E_U[\hat{n}] \quad (4)$$

where ρ denotes the charge density and \hat{n} is the TM on-site 3d occupation matrix. For these states the Hubbard interaction term E_{Hub} replaces the LDA energy contribution E_{dc} . The U correction term $E_U \equiv E_{\text{Hub}} - E_{\text{dc}}$ is defined by Eq. 4. Although E_{dc} is not uniquely defined, we have chosen the spherically averaged version³³ due to the considerations discussed in Ref. 25. Therefore

$$E_{\text{dc}}(\hat{n}) = \frac{U - J}{2} \text{Tr} \hat{n} (\text{Tr} \hat{n} - 1) = \frac{U_{\text{eff}}}{2} \text{Tr} \hat{n} (\text{Tr} \hat{n} - 1), \quad (5)$$

$$E_U(\hat{n}) = \frac{U - J}{2} \text{Tr} (\hat{n}(1 - \hat{n})) = \frac{U_{\text{eff}}}{2} \text{Tr} (\hat{n}(1 - \hat{n})), \quad (6)$$

where we have defined the effective interaction parameter $U_{\text{eff}} = U - J$, or simply U afterwards. The calculated energies are insensitive to the J parameter at fixed U_{eff} ²⁵ and we include it in U_{eff} .

D. Self-consistent Calculation of effective U

We determine the U parameter using the method presented in²⁶ which we briefly outline below. This method is based on calculating the response in the occupation of TM states to a small perturbation of their local potential.

We start from an LDA/GGA ($U = 0$) calculation as the reference point. Then a small perturbation

$$dV = \alpha P_d^i \quad P_d^i = \sum_{m=-2}^2 |m^i\rangle\langle m^i|$$

in the local d-orbital potential is exerted on metal site i , where P_d^i represents the projector on the d states manifold of ion i , and α is the amplitude of the potential shift applied to the d levels. This induces a change in the occupation number of ion i as well as other ions. Thus we can calculate directly the response matrices,

$$\chi_{ji} = \frac{dn_d^j}{d\alpha_i}; \quad \chi_{0ji} = \frac{dn_{0d}^j}{d\alpha_i}, \quad (7)$$

which measure the variation of the d -manifold charge density n_d^j , on ion j , produced by a potential shift at ion i . The subscript “0” denotes the bare response, calculated without self-consistency (the Kohn-Sham potential apart from dV is frozen at the value obtained in LDA/GGA before the perturbation), and χ_{ji} is the screened response (charge density and potential relaxed). The effective interaction parameter U is then obtained as

$$U = (\chi_0^{-1} - \chi^{-1})_{ii}. \quad (8)$$

This result is reminiscent of the well known Random Phase Approximation in linear response theory, in which the Coulomb interaction kernel is given as a difference among the interacting density response and the non-interacting one³⁴. As we use the integrated quantity n_d^i to probe the responses, the calculated effective interaction is averaged over the ion in the same spirit as DFT+ U . The matrix in Eq. 8, whose diagonal term defines the on-site Hubbard U , also contains non-diagonal terms corresponding to inter-site effective interactions in LDA/GGA. These are not used in the DFT+ U model. This method to compute U is based on the full account of the screening to the external perturbation operated by the electron-electron interaction. We also notice that the calculation of U is based on the use of the same occupancy matrices entering the DFT+ U functional and this guarantees full consistency with the calculation we perform²⁶

III. DETAILS OF THE CALCULATION AND RESULTS

Total energy calculations were performed for Ni, Mn, Co and Fe in the olivines, layered and spinel structures whenever experimental information on the voltage is available. For each system the total energy of the lithiated and delithiated state was calculated with GGA and GGA+ U , with the projector-augmented wave (PAW) method^{35,36} as implemented in the Vienna Ab-initio Simulation Package³⁷. The use of GGA over LDA has previously been shown to be essential for correctly reproducing magnetic interactions and possible Jahn-Teller distortions³⁸. An energy cut-off of 500 eV and appropriate k -point mesh were chosen so that the total ground state energy is converged to within 3meV per FU. All the atoms and cell parameters of each structure are fully relaxed. Jahn-Teller distortions are allowed where the transition metal ions are Jahn-Teller active (Mn³⁺ and Ni³⁺ in our case) by explicitly breaking the symmetry of the unit cell. Our relaxed cells of layered LiNiO₂ and spinel Li₂Mn₂O₄ agree well with the calculations in Ref. 39 on Jahn-Teller distorted systems using GGA. All calculations are performed with spin-polarization. As discussed later, the total energy of a given structure depends critically on the magnetic state of the metal ions, and high-spin states are favored by the DFT+ U scheme we used. The ordering of the spin on the ions in different magnetic structures (i.e. ferromagnetic, antiferromagnetic or more complicated ordering) results in difference in the total energy of the order 10–60 meV per formula unit. From the total energies, the average lithiation potential can be calculated through equation 3.

Table II shows the self-consistently calculated effective U for Mn, Fe, Co and Ni in different valence states and structures. For each structure, the U for the low and high valence states were respectively calculated in a fully lithiated and de-lithiated structure. In all cases, except Ni³⁺/Ni⁴⁺ in the layered structure, a higher valence state leads to a higher U . For the three cases (Mn³⁺/Co³⁺/Ni³⁺) for which we have a U in a close-packed (layered or spinel) oxides and in an olivine phosphate structure, the U is higher for the olivine structure. This may be related to the fact that the TM-octahedra in the olivine are only corner sharing in two directions but separated from each other by phosphate groups in the third direction, leading to very narrow bandwidth and well localized TM- d states. For comparison we also list the U values calculated in Ref. 40 for TM monoxides MO (M = Mn, Fe, Co and Ni) in non spin-polarized state. Good agreement with LiMPO₄ is found except

for Fe^{2+} . The possible reason for this discrepancy could be a slightly different definition of the interaction parameter U . In Ref. 40 $U = U_K + U_P$ where U_P comes from the potential energy contribution to the response of the system, and U_K is the free-electron-like term (kinetic energy contribution). In our calculation, instead, the U_K term, which is not related to the electron-electron interaction, has been properly removed by subtracting $-\chi_0^{-1}$ from the total response of the system. Our U thus corresponds to the U_P term of Ref. 40.

	Mn^{2+}	Mn^{3+}	Mn^{4+}	Fe^{2+}	Fe^{3+}	Co^{2+}	Co^{3+}	Co^{4+}	Ni^{2+}	Ni^{3+}	Ni^{4+}
Olivine	3.92	5.09		3.71	4.90	5.05	6.34		5.26	6.93	
Layered							4.91	5.37		6.70	6.04
Spinel		4.64	5.04				5.62	6.17			
Monoxide ⁴⁰	3.6			4.6		5.0			5.1		

TABLE II: Calculated U in eV.

Figure 4 and 5 show respectively the average Li insertion voltage as function of U in the olivine, and in the layered and spinel structure. The horizontal short line indicates the experimentally measured voltage. Three calculated points for each system are marked on the curve: the small open circles indicate respectively the voltage one would obtain using the calculated U for the most reduced and most oxidized TM-state in each structure (e.g. Fe^{2+} and Fe^{3+} in LiFePO_4). The large filled circle corresponds to the voltage for the averaged U . The results for each system are discussed in more detail below.

A. Olivine structures Li_xMPO_4 (M=Mn, Fe, Co, Ni)

According to neutron-diffraction experiments^{41,42} the magnetic ordering of LiMPO_4 is antiferromagnetic (AFM) within the approximately square lattice of metal ions for each of the above four TM. FePO_4 is also found to have AFM magnetic ordering⁴². The results in Fig. 4 have been calculated with AFM spin configuration in both end members. The calculated and experimental cell parameters, as well as the electronic occupation of the TM ions are listed in Table III.

Mn Both Mn^{2+} and Mn^{3+} are high-spin ions in GGA and GGA+ U calculations. Attempts to constrain them to lower spin states lead to much higher energy. FM ordered

		a (Å)	b (Å)	c(Å)	V(Å ³)	TM ion config.
LiMnPO ₄	GGA	10.55	6.13	4.78	309.13	$t_{2g}^3 e_g^2$
	GGA+ <i>U</i>	10.62	6.17	4.80	314.52	$t_{2g}^3 e_g^2$
	Exp. ³⁰	10.44	6.09	4.75	302.00	
MnPO ₄	GGA	9.92	6.01	4.93	293.92	$t_{2g}^3 e_g^1$
	GGA+ <i>U</i>	9.98	6.07	4.96	300.47	$t_{2g}^3 e_g^1$
	Exp. ³⁰	9.69	5.93	4.78	274.67	
LiFePO ₄	GGA	10.39	6.04	4.75	298.09	$t_{2g}^4 e_g^2$
	GGA+ <i>U</i>	10.42	6.07	4.76	301.07	$t_{2g}^4 e_g^2$
	Exp. ²⁷	10.33	6.01	4.69	291.39	
FePO ₄	GGA	9.99	5.93	4.90	290.28	$t_{2g}^3 e_g^2$
	GGA+ <i>U</i>	9.99	5.88	4.87	286.07	$t_{2g}^3 e_g^2$
	Exp. ²⁷	9.82	5.79	4.79	272.36	
LiCoPO ₄	GGA	10.30	5.93	4.75	290.13	$t_{2g}^5 e_g^2$
	GGA+ <i>U</i>	10.33	5.97	4.76	293.55	$t_{2g}^5 e_g^2$
	Exp. ³¹	10.20	5.92	4.70	283.90	
CoPO ₄	GGA	9.71	5.48	4.59	244.24	t_{2g}^6
	GGA+ <i>U</i>	9.98	5.78	4.74	273.42	$t_{2g}^4 e_g^2$
	Exp. ³¹	10.09	5.85	4.72	278.66	
LiNiPO ₄	GGA	10.09	5.91	4.74	282.66	$t_{2g}^6 e_g^2$
	GGA+ <i>U</i>	10.12	5.90	4.73	282.42	$t_{2g}^6 e_g^2$
	Exp. ⁴³	10.03	5.85	4.68	274.49	
NiPO ₄	GGA	9.66	5.72	4.71	260.25	$t_{2g}^6 e_g^1$
	GGA+ <i>U</i>	9.92	5.82	4.84	279.43	$t_{2g}^6 e_g^1$

TABLE III: Cell parameters of the olivine structures in the lithiated and de-lithiated states, as well as the corresponding electron configuration at the TM ions.

magnetic structures are 10 - 30meV higher in energy than the AFM ordered magnetic structure as *U* is varied. A strong collective Jahn-Teller distortion is observed in MnPO₄, where Mn³⁺ is in the high spin $t_{2g}^3 e_g^1$ state, in GGA(+*U*). The experimental voltage for the MnPO₄/LiMnPO₄ redox couple has been obtained from³⁰. The voltage

predicted with GGA+ U (4.04V at $U = (U_{\text{Mn}^{2+}} + U_{\text{Mn}^{3+}})/2$) is within a few % of the experimental voltage (4.1V), and in sharp contrast to the large error made by GGA ($V_{\text{GGA}} = 2.98\text{V}$).

Fe Both Fe^{2+} and Fe^{3+} are high-spin in GGA(+ U) calculations, and the AFM ordering is more stable than FM ordering. Using $U_{\text{Fe}^{2+}}$ and $U_{\text{Fe}^{3+}}$ we calculated a voltage of 3.39 and 3.55V respectively. The voltage calculated with the average U ($= 4.30\text{eV}$) is 3.47V , which agrees very well with the experimentally measured value of 3.5V ²⁴. This is a substantial improvement over the GGA predicted value of 2.97V . Previously, the localization of electrons induced by U was also shown to qualitatively affect the phase behavior in this system²⁵.

Co In LiCoPO_4 Co^{2+} is stable in the high-spin $t_{2g}^5e_g^2$ state. In the delithiated CoPO_4 , Co^{3+} is stable as non spin-polarized with GGA, but more stable by several eV with GGA+ U in the high spin $t_{2g}^4e_g^2$ configuration at the calculated U value of 6.34eV . As shown in Table III the cell parameters of CoPO_4 calculated with non spin-polarized Co^{3+} in GGA is appreciably smaller than experimental values, while GGA usually slightly overestimates cell parameters. With GGA+ U and high-spin Co^{3+} the calculated parameters are close to experimental values. While there is only limited electrochemical data on this material²⁷, the predicted voltage of 4.73V at U_{average} is within a few % of the result 4.8V established by Anime *et. al*³¹, compared to the poor GGA prediction of 3.70V . The high voltage of this material makes it particularly attractive for high-energy density applications.

Ni Though LiNiPO_4 has been synthesized, no Li can be removed from it electrochemically⁴⁴. Hence the voltage is probably larger than 5V , the limit of most electrolyte systems. At $x = 1$ Ni^{2+} is stable as high-spin $t_{2g}^6e_g^2$. At $x = 0$ Ni^{3+} occurs in the low spin state $t_{2g}^6e_g^1$ for both GGA and GGA+ U , but the high spin state $t_{2g}^5e_g^2$ is less unstable in GGA+ U than in GGA. Note that low-spin Ni^{3+} is a weak Jahn-Teller ion, and no appreciable collective distortion is observed in our relaxed unit cell. With U_{average} , a voltage of 5.07V is obtained, which is in agreement with the fact that no Li can be removed from this material.

B. Layered Li_xMO_2 (M=Co, Ni)

For the layered and spinel structures AFM spin ordering on transition metal ions is topologically frustrated, and their actual magnetic ground states are not always clear in experiment. But as the energy associated with different magnetic orderings is small, the simple FM ordering is used in the following calculations.

Co In LiCoO_2 Co^{3+} is stable in the non spin-polarized state for the calculated $U_{\text{Co}^{3+}} = 4.91\text{eV}$. At $x = 0$, Co^{4+} is almost degenerate in either non spin-polarized or spin-polarized t_{2g}^5 in GGA, but more stable with spin-polarization in GGA+U at the calculated $U_{\text{Co}^{4+}} = 5.37\text{eV}$. While GGA+U still improves the agreement of voltage with experiment²³ over pure GGA, the error for this system is larger than in the other systems we calculated. While we have no obvious explanation for this, it might be related to the fact that the pure GGA result is already closer to experiment than for all other systems.

Ni In LiNiO_2 Ni^{3+} is most stable in the low-spin $t_{2g}^6 e_g^1$ state and is a weak Jahn-Teller ion. With GGA a distorted unit cell is found with the short and the long Ni-O bond length being 1.92\AA and 2.13\AA , respectively, compared to experimental values of 1.91\AA and 2.14\AA ³⁹, and a stabilization energy relative to an undistorted cell of only -2meV , within the range of numerical errors, compared to -11meV in³⁹. With GGA+U no appreciable distortion is observed. Experimentally there is no cooperative Jahn-Teller distortion in LiNiO_2 though the Ni-O octahedra are locally Jahn-Teller distorted⁴⁵, suggesting a very small stabilization energy, not inconsistent with both GGA and GGA+U results. At $x = 0$, Ni^{4+} is stable as a non spin-polarized ion. The GGA+U voltage value of 3.92V agrees well with the experimental average voltage of 3.85V ²², and is substantially better than the pure GGA result of 3.19V .

C. Spinel $\text{Li}_x\text{M}_2\text{O}_4$ (M=Mn, Co)

For the spinel $\text{Li}_x\text{Mn}_2\text{O}_4$ there are two distinct plateaus in the voltage profile, between $0 < x < 1$ and $1 < x < 2$, respectively. For $0 < x < 1$ Li enters tetrahedral sites, while the reaction from LiMn_2O_4 to $\text{Li}_2\text{Mn}_2\text{O}_4$ occurs through a two-phase process whereby the LiMn_2O_4 phase with only tetrahedral Li disappears at the expense of the $\text{Li}_2\text{Mn}_2\text{O}_4$ phase

with all Li octahedral. Calculations were done for $x = 0, 1$ and 2 structures to get separate average voltage values for the two processes. For $M = Co$ the $0 < x < 1$ reaction potential curve is difficult to obtain accurately in experiments. Therefore only the average voltage for the $1 < x < 2$ reaction is shown in fig. 5.

Mn Both Mn^{4+} and Mn^{3+} are high-spin. Mn^{3+} is a strong Jahn-Teller active ion. In GGA, the calculated Mn-O short and long bond lengths 1.94\AA and 2.40\AA agree with Ref. 39; in GGA+ U they become 1.96\AA and 2.32\AA , respectively. Experimental values are 1.94\AA and 2.29\AA , respectively⁴⁶, showing that the good structural prediction of GGA is retained in GGA+ U . Coexistence of distinct Mn^{4+} and Mn^{3+} is found in GGA+ U in the LiM_2O_4 compound. The GGA+ U_{average} results (4.19V and 2.97V respectively, for the first and second plateaus) is in excellent agreement with the experimentally measured values of 4.15V and 2.95V ²³.

Co Like in the layered structure, Co^{3+} in $Li_2Co_2O_4$ is non spin-polarized, and at $x = 0$ Co^{4+} is more stable as spin polarized t_{2g}^5 in GGA+ U . The GGA+ U voltage (3.56V at $U_{\text{average}} = 4.84\text{eV}$) agrees very well with experimental data available for the $Li_1Co_2O_4$ to $Li_2Co_2O_4$ reaction (3.5V ³²).

Note that in the $x = 1$ structure of the spinel materials $Li_xM_2O_4$ we find distinct M^{3+} and M^{4+} ions in GGA+ U instead of ions of intermediate valence. The same phenomenon was observed in the intermediate structures Li_xFePO_4 of the iron phosphate²⁵. This is a direct consequence of the E_U correction term to the total energy in Eq. 4 which penalizes the non-integral occupation of the d -orbitals. Such charge ordering is necessary for correctly predicting the $0 < x < 1$ and $1 < x < 2$ average voltage values of $Li_xMn_2O_4$ simultaneously, as well as the $1 < x < 2$ voltage of $Li_xCo_2O_4$, and is not present in pure GGA unless localization is assisted by a strong polaronic contribution such as the Jahn-Teller distortion around Mn^{3+} .

IV. DISCUSSION

Introduction of Coulombic on-site correlations in GGA through the GGA+ U clearly improves predicted lithiation potentials considerably over the use of pure GGA (or LDA for that matter). The errors of GGA+ U and pure GGA on all systems for which we have

experimental data are summarized in Fig. 6. Pure GGA consistently underestimates the lithiation voltage, which is a measure of the energy lowering when Li is transferred from Li metal (the anodic reference) to a Li^+ ion and electron in the TM oxide or phosphate. The contribution of the Li^+ ion to the reaction energy is largely electrostatic, and one would expect this effect to be well captured in GGA or LDA. Hence, the large voltage error in LDA/GGA must arise from the electron transfer from Li metal to the TM cation. Since the voltage is always underestimated in LDA/GGA these approximations clearly penalize the energy of the electron on the TM, thereby lowering the reaction energy. It seems reasonable to attribute this to the poor treatment of electronic correlations in LDA/GGA. In metallic lithium the electron is affected by a small self-interaction in LDA/GGA as its charge density is delocalized. On the TM ion, however, the electron occupies a much more localized d -orbital and will experience a much larger self-interaction. The lack of cancellation between the self-interactions contributions to the energy, which are related to an improper description of the correlation effects in LDA/GGA, leads to a systematic error in the prediction of the redox potential. In the direction in which the electron is transferred from a delocalized to a localized state, the reaction energy is penalized (not negative enough), making the potential too small. The use of GGA+ U allows for a better description of the electronic correlation and, by discouraging fractional occupations of the Kohn-Sham orbitals, removes the spurious self-interaction thus producing a much more accurate prediction of the redox voltage. While we demonstrate the GGA/LDA problem and improvement obtained with DFT+ U on Li-insertion materials, we believe that a more accurate description of correlation effects within the DFT+ U scheme is also necessary in the study of other redox processes in which electrons are transferred between states of different kind (e.g. catalysis of organic molecules on TM surfaces). In fact, as explained in Ref. 26, a better description of the electronic correlation (which enforces the independence of the single electron energy eigenvalues of the partially occupied states on their occupation, thus leading to the elimination of the spurious self-interaction) is needed to reproduce the physical difference among the ionization potential and the electronic affinity (or the band gap in crystalline solids) which plays a very important role in the energetics of processes involving electron transfer.

In our calculations high-spin TM ions are always energetically favored by GGA+ U over low-spin or non spin-polarized states. In CoPO_4 the non spin-polarized Co^{3+} in GGA leads to cell parameters inconsistent with experiment. In GGA+ U Co^{3+} becomes high spin,

improving agreement with experiment. For the other systems the GGA and GGA+ U cell parameters are rather close, though GGA+ U seems to lead to volumes that are slightly too high. Jahn-Teller distortions predicted by GGA are also reproduced in GGA+ U for Mn³⁺.

In summary, we have shown that the under-estimation of the lithium intercalation voltage in LDA/GGA can be corrected by using GGA+ U with a self-consistently calculated parameters U , without sacrificing properties that are already accurately predicted by GGA (e.g. Jahn-Teller effect, cell parameters, magnetic ordering). Voltages for most systems are predicted within a few % of experimental values.

We believe that DFT+ U will significantly improve the accuracy with which the voltage for candidate materials can be predicted, and therefore enhance the capability of screening new materials for their ability to be good cathodes.

Acknowledgments

This work was supported by the Department of Energy under Contract number DE-FG02-96ER45571 and by the MRSEC program of the National Science Foundation under contract number DMR-0213282.

¹ V. I. Anisimov, J. Zaanen, and O. K. Andersen, Phys. Rev. B **44**, 943 (1991).

² V. I. Anisimov, I. V. Solovyev, M. A. Korotin, et al., Phys. Rev. B **48**, 16929 (1993).

³ A. I. Liechtenstein, V. I. Anisimov, and J. Zaanen, Phys. Rev. B **52**, R5467 (1995).

⁴ M. K. Aydinol, A. F. Kohan, G. Ceder, K. Cho and J. Joannopoulos, Phys. Rev. B, **56**, 1354 (1997).

⁵ C. Wolverton and A. Zunger, J. Electrochem. Soc. **145**, 2424 (1998).

⁶ M. Launay, F. Boucher, P. Gressier and G. Ouvrard, J. Solid State Chem. **176**, 556 (2003).

⁷ P. Tang and N. A. W. Holzwarth, Phys. Rev. B, **68**, 165107 (2003).

⁸ B. J. Hwang, Y. W. Tsai, D. Carlier and G. Ceder, Chem. Materials, **15**, 3676 (2003).

⁹ X. Rocquefelte, F. Boucher, P. Gressier and G. Ouvrard, Chem. Materials, **15**, 1812 (2003).

¹⁰ K. R. Kganyago, P. E. Nguope and C. R. A. Catlow, Solid State Ionics **159**, 21 (2003).

¹¹ R. Prasad, R. Benedek and M. M. Thackeray, B. Mater. Sci. **26**, 147 (2003).

¹² Y. Koyama, I. Tanaka and H. Adachi, Adv. Quant. Chem. **42**, 145 (2003).

¹³ D. Morgan, G. Ceder, M. Y. Saidi, J. Barker, J. Swoyer, H. Huang and G. Adamson, Chem. Mater. **14**, 4684 (2002).

¹⁴ M. L. Doublet, F. Lemoigno, F. Gillot and L. Monconduit, Chem. Mater. **14**, 4126 (2002).

¹⁵ A. Van der Ven, M. K. Aydinol and G. Ceder, J. Electrochem. Soc. **145**, 2149 (1998).

¹⁶ I. A. Courtney, J. S. Tse, O. Mao, J. Hafner, and J. R. Dahn, Phys. Rev. B, **58**, 15583 (1998).

¹⁷ A. Van der Ven, M. K. Aydinol, G. Ceder, et al, Phys. Rev. B **58**, 2975 (1998).

¹⁸ M. E. Arroyo y de Dompablo, A. Van der Ven and G. Ceder, Phys Rev B **66**, 064112 (2002).

¹⁹ J. Reed, G. Ceder, A. Van der Ven, Electrochem. and Solid State Lett. **4**, A78 (2001).

²⁰ A. Van der Ven and G. Ceder, Electrochem. and Solid State Lett. **3**, 301 (2000).

²¹ D. Morgan, G. Ceder, M. Y. Saidi, et al, J. Power Sources, **119**, 755 (2003).

²² C. Delmas, M. Menetrier, L. Croguennec, et al, Intl. J. Inorg. Materials **1**, 11 (1999).

²³ T. Ohzuku and A. Ueda, Solid State Ionics **69**, 201 (1994).

²⁴ A. Yamada, S. C. Chung and K. Hinokuma, J. Electrochem. Soc. **148**, A224 (2001).

²⁵ F. Zhou, C. A. Marianetti, M. Cococcioni, D. Morgan, G. Ceder, Phys. Rev. B, **69**, 201101 (2004).

²⁶ M. Cococcioni, PhD thesis, International School for Advanced Studies (SISSA) (2002), available

at <http://www.sissa.it/cm/phd.php>; M. Cococcioni and S. de Gironcoli, cond-mat/0405160, submitted for publication.

²⁷ A. K. Padhi, K. S. Nanjundaswamy, and J. B. Goodenough, *J. Electrochem. Soc.* **144**, 1188 (1997).

²⁸ For review see M. M. Thackeray, *J. Electrochem. Soc.* **142**, 2558 (1995) and references therein.

²⁹ W. R. McKinnon, Insertion electrodes I: Atomic and electronic structure of the hosts and their insertion compounds. In P. G. Bruce, editor, *Solid state electrochemistry*, volume 16, pages 163–198, Cambridge, 1995. Cambridge University Press.

³⁰ G. Li, H. Azuma and M. Tohda, *Electrochem. and Solid State Lett.* **5**, A135 (2002).

³¹ K. Amine, H. Yasuda and M. Yamachi, *Electrochem. and Solid State Lett.* **3**, 178 (2000),.

³² S. Choi and A. Manthiram, *J. Electrochem. Soc.* **149**, A162 (2002).

³³ S. L. Dudarev, G. A. Botton, S. Y. Savrasov, C. J. Humphreys and A. P. Sutton, *Phys. Rev. B* **57**, 1505 (1998).

³⁴ S. L. Adler, *Phys. Rev.* **126**, 413 (1962); N. Wiser, *Phys. Rev.* **129**, 62 (1963).

³⁵ P. E. Blöchl, *Phys. Rev. B* **50**, 17953 (1994).

³⁶ G. Kresse, and D. Joubert, *Phys. Rev. B* **59**, 1758 (1999).

³⁷ G. Kresse and J. Furthmüller, *Phys. Rev. B* **54**, 11169 (1996); *Comput. Mater. Sci.* **6**, 15 (1996).

³⁸ S. K. Mishra and G. Ceder, *Phys. Rev. B* **59**, 6120 (1999).

³⁹ C. A. Marianetti, D. Morgan, G. Ceder, *Phys. Rev. B* **63**, 224304(2001).

⁴⁰ W. E. Pickett, S. C. Erwin, and E. C. Ethridge, *Phys. Rev. B* **58**, 1201(1998).

⁴¹ R. P. Santoro, D. J. Segal and R. E. Newman, *J. Phys. Chem. Solids* **27**, 1192 (1966); R. P. Santoro and R. E. Newnham, *Acta Cryst.* **22**, 344 (1967).

⁴² G. Rousse, J. Rodriguez-Carvajal, S. Patoux, and C. Masquelier, *Chem. Mater.* **15**, 4082 (2003) and the references therein.

⁴³ O. García-Moreno, M. Alvarez-Vega, F. García-Alvarado, J. García-Jaca, J.M. Gallardo-Amores, M.L. Sanjuán, and U. Amador, *Chem. Mater.* **13**, 1570 (2001).

⁴⁴ S. Okada, S. Sawa, M. Egashira, et al., *J. Power Sources* **97-8**, 430 (2001).

⁴⁵ A. Rougier, C. Delmas, and A. V. Chadwick, *Solid State Commun.* **94**, 123 (1995).

⁴⁶ R. Hoppe, G. Brachtel, and M. Jansen, *Z. Anorg. Allg. Chem.* **417**, 1 (1975).

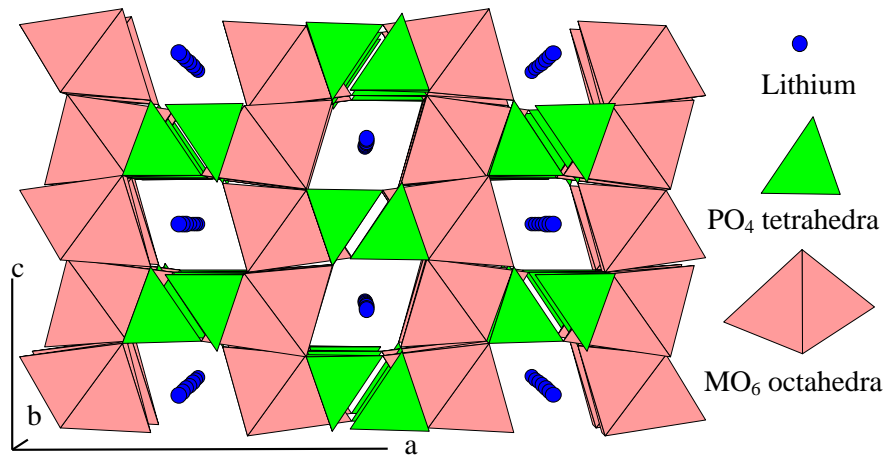


FIG. 1: The olivine structure with cation polyhedra.

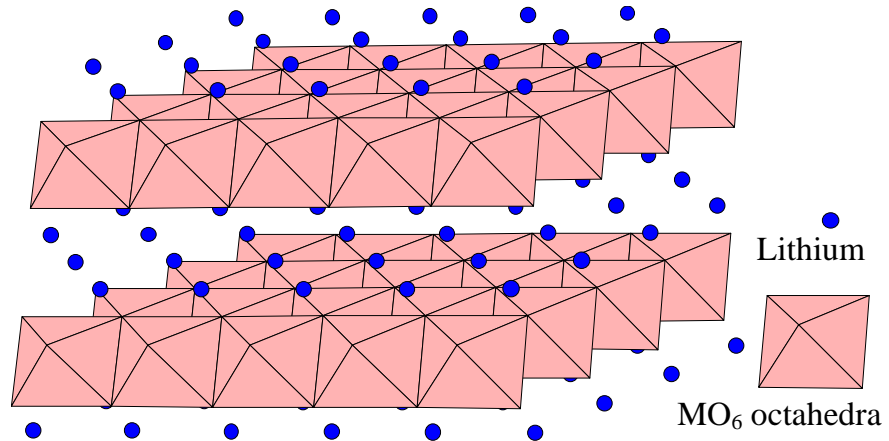


FIG. 2: The layered structure with MO_6 octahedra and lithium atoms.

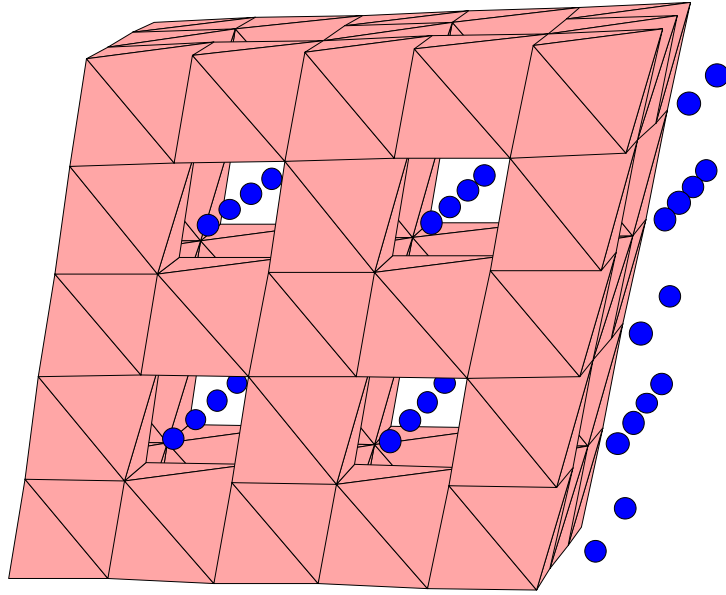


FIG. 3: The spinel-like structure when fully lithiated ($x = 2$, Li atoms taking octahedral positions) with MO_6 octahedra and lithium atoms.

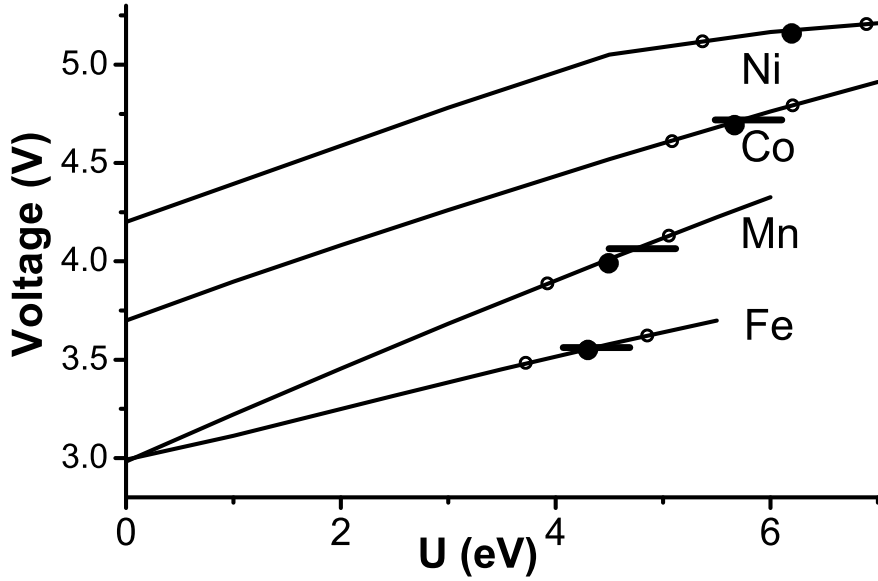


FIG. 4: Voltage as a function of U for the LiMPO_4 materials in the olivine structure. The short horizontal lines on the curves indicate the experimental voltage of the each material (no experimental information is available for LiNiPO_4). The two small open circles on a curve represent the voltage for U calculated in the oxidized (delithiated) or reduced (lithiated) states. The big solid circle represents the voltage at the average of the two U values.

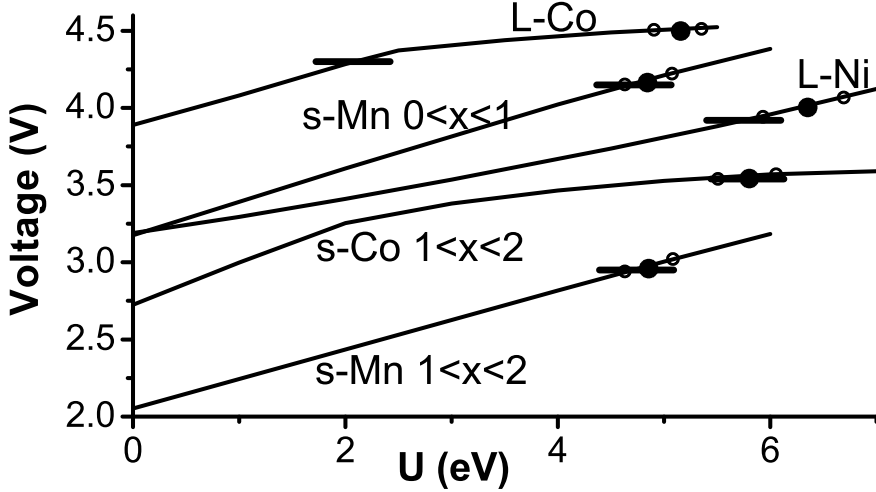


FIG. 5: Voltage as a function of U for the layered and spinel structures. Legend the same as in Fig. 4.

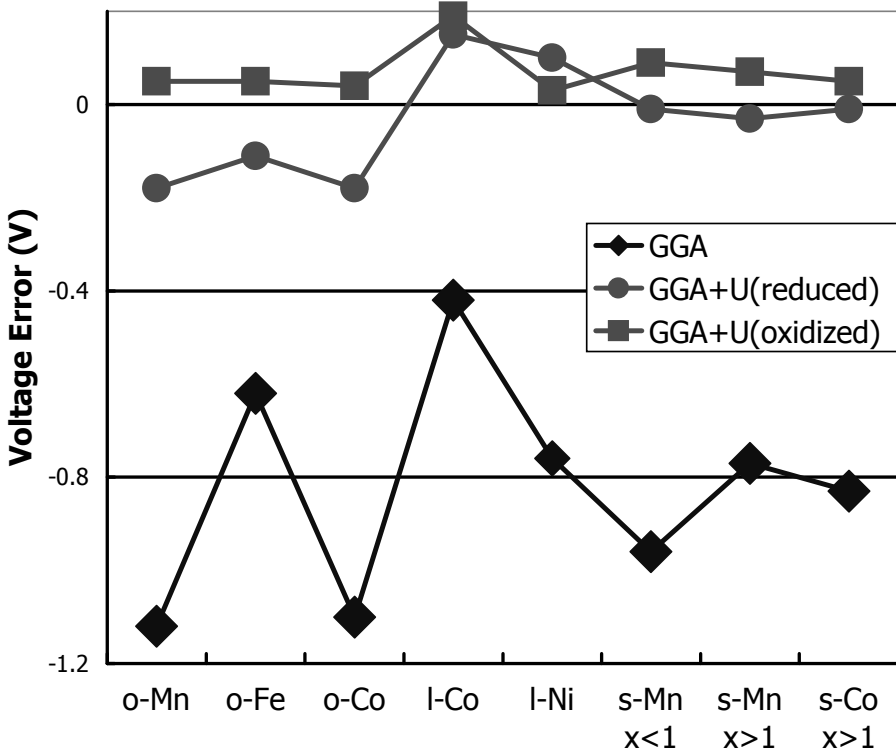


FIG. 6: Difference between calculated and experimental voltage [5-9], for GGA and GGA+U, at the calculated U of the oxidized (delithiated) and reduced (lithiated) states, respectively (l=layered, s=spinel). For the spinel structures two voltage values for the $0 < x < 1$ and $1 < x < 2$ plateaus are calculated separately. Olivine LiNiPO_4 is not shown here because the voltage is unknown.